Acoustics 2021
Wollongong, Australia
MAKING WAVES

Prediction of Vortex-Shedding Noise from Flow Over a High Aspect Ratio Cylinder Using an Acoustic Analogy

William Sidebottom (1,2), Paul Croaker (1), David Jones (1) and Mattias Liefvendahl (3)

(1) Maritime Division, Defence Science and Technology Group, Melbourne, Australia
(2) Mechanical and Manufacturing Engineering, University of New South Wales, Sydney, Australia
(3) Division 3, Swedish Defence Research Agency (FOI), Kista, Sweden

ABSTRACT

Noise generated by turbulent flow over high-aspect ratio bluff bodies is of interest in many engineering applications including the design wind turbines, aircraft and marine vessels. This study investigates the noise produced by a large span circular cylinder in cross-flow at a Reynolds number based on diameter (Re_D) of 2.2×10^4. Large eddy simulations and the Ffowcs Williams and Hawkings acoustic analogy were used to simulate the aerodynamic and aeroacoustic fields around both full- and reduced-span cylinders, with aspect ratios of 18.75 and 4.0 respectively. At Re_D=2.2×10^4, there is well-documented evidence of a low-frequency modulation of the fluctuating lift force, which is evident in the present results. The modulation means that very long runtimes are required to reach statistical convergence for the full-span cylinder. The modulation is not observed in the reduced-span simulation results, which significantly reduces the time taken to reach statistical convergence. The sound pressure levels (SPL) predicted from the full-span simulation are consistently 3-6 dB below experimental values. The SPLs predicted by scaling the reduced span simulation were in better agreement with the measured values, particularly around the vortex shedding frequency. These results show that more accurate far-field acoustic predictions can be obtained by scaling the results from the reduced-span simulation, when compared to the full-span predictions.

1 INTRODUCTION

Flow over a circular cylinder is commonly used in fluid dynamics to test numerical methods. This is primarily due to the simple geometry, the many interesting flow phenomena that occur both near the surface of the cylinder and in its wake, and the availability of experimental and numerical data for comparison. In this study, large-eddy simulations (LES) are used in conjunction with an acoustic analogy to predict the far-field acoustic signature produced by flow over a cylinder at a Reynolds number based on diameter, Re_D, of 2.2×10^4 (where $Re_D = U_\infty D/\nu$, U_∞ is the freestream velocity, D is the diameter of the cylinder, and ν is the kinematic viscosity). The predominant noise source at this Reynolds number is vortex shedding.

Previous studies (Bensow & Liefvendahl, 2016; Liefvendahl & Bensow, 2018) have used a similar combination of LES and an acoustic analogy to predict the far-field sound radiated by flow over a cylinder at $Re_D = 4.0 \times 10^4$. Numerical predictions of the sound pressure level from these studies were in good agreement with the experimental results of Latorre-Iglasias et al. (2016). The measurements from this experiment were limited to only one radiation direction, being perpendicular to the flow and oriented in the direction of the lift force. The experiment outlined by Casalino & Jacob (2003) investigated flow over a cylinder at $Re_D = 2.2 \times 10^4$ and provided far-field sound measurements at a range of observation angles. At this Reynolds number the flow around the cylinder is sub-critical with laminar boundary layers on the cylinder surface. Boundary layer separation, shear layer growth and instability then lead to the creation of discrete vortices that are shed from the cylinder and create unsteady lift and drag forces and transition to turbulence in the wake.

Numerical studies that have considered the experimental arrangement of Latorre-Iglasias et al. (2016) have been based on simplified two-dimensional RANS (Reynolds-averaged Navier-Stokes) methods. They have necessarily included statistical models and information from the experiment about the coherence properties to reproduce the three-dimensionality of the flow (Latorre-Iglasias et al. 2016; Doolan, 2010). The results in both of these studies show good agreement with the experimental data at the tonal frequencies. The approach used in the present simulations, which is similar to that presented by Liefvendahl & Bensow (2018), simulates the full three-dimensional problem without the need for any assumptions regarding the statistics of the flow, or for any input from experimental measurements.

Due to the high aspect ratio of 18.75 for the full-span cylinder, there is a low-frequency modulation of the amplitude of the unsteady lift force acting on the cylinder. This modulation is also apparent in the surface pressures and associated far-field sound pressure. Casalino and Jacob (2003) propose that this amplitude modulation is caused by oblique vortex shedding which introduces a spanwise variation in the vortex shedding phase. A common technique to approximate the sound from long-span bodies using numerical techniques involves predicting the sound from a reduced-span model and then applying a correction based on the spanwise coherence length to approximate the sound from the full-span body. In the present study, the method outlined by Seo & Moon (2007) is used to correct the results from reduced-span simulations.

2 NUMERICAL METHODS

The computational aeroacoustics method employed here consists of an incompressible LES of the flow around the cylinder and an acoustic analogy to predict the far-field acoustic pressure. The source terms for the acoustic analogy are obtained from the flow around the cylinder.

The turbulence closure used to solve the incompressible Navier-Stokes equations (NSE) in the LES framework was the wall-adapting local eddy (WALE) viscosity model (Nicoud & Ducros, 1999). This model was chosen because it displays the correct behaviour in the near-wall region (*i.e.* the turbulent viscosity goes to zero at the wall), making it applicable for wall-bounded flows. Second-order accurate differencing schemes were used to discretise the convective and time-dependant terms in the NSE. All simulations were calculated using the open-source computational fluid dynamics software package OpenFOAM (Weller et al., 1998). The far-field noise was calculated using the Ffowcs-Williams and Hawkings acoustic analogy (Ffowcs-Williams & Hawkings, 1969).

Simulations for both the full-span and reduced-span cylinders were run for a non-dimensional time, $T = tU_\infty/D$, of 625, with statistics calculated over a period of $T = 560$ (here, t is the time in seconds). This corresponds to approximately 13 domain transit times or 125 shedding cycles. The chosen time step, $\Delta t = 2.5 \times 10^{-7}$, resulted in approximately 16,000 time steps per shedding cycle.

2.1 Geometry

The geometry was chosen to match the experimental setup by (Casalino & Jacob, 2003). In this, a cylinder with diameter, $D = 0.016$ m, and length, $L = 0.3$ m, was fixed between two parallel rectangular end plates and placed in the potential core of a partially flanged rectangular jet. The inflow velocity was 20 m/s, corresponding to a Reynolds number based on the diameter of 2.2×10^4 and a Mach number of 0.06. Acoustic measurements were taken at a distance $r = 1.38$ m from the cylinder mid-point at various observation angles.

The dimensions of the domain for the full-span simulation are shown in Figure 1(a), and those for the reduced-span simulation are shown in Figure 1(b). For the full-span simulation, a no-slip boundary condition was used on the end plates, where a periodic boundary condition was used on the corresponding surfaces in the reduced-span simulation. The mesh of the full-span cylinder consisted of 139 million cells, with the first off-wall grid point placed at $y^+ \approx 1$ (here, $y^+ = yu_\tau/\nu$, where y is the wall-normal coordinate, and $u_\tau = \sqrt{\tau_w/\rho}$ is the friction velocity given in terms of the wall shear-stress, τ_w, and the density, ρ). The reduced-span mesh consisted of 30 million cells and had the same cell sizes as the full-span mesh. The length of the cylinder in the reduced-span simulation was reduced to 0.064 m. The locations of the microphones for both the full-span and the reduced-span simulations are also shown in Figure 1. These are the same locations as those that were used by (Casalino & Jacob, 2003).

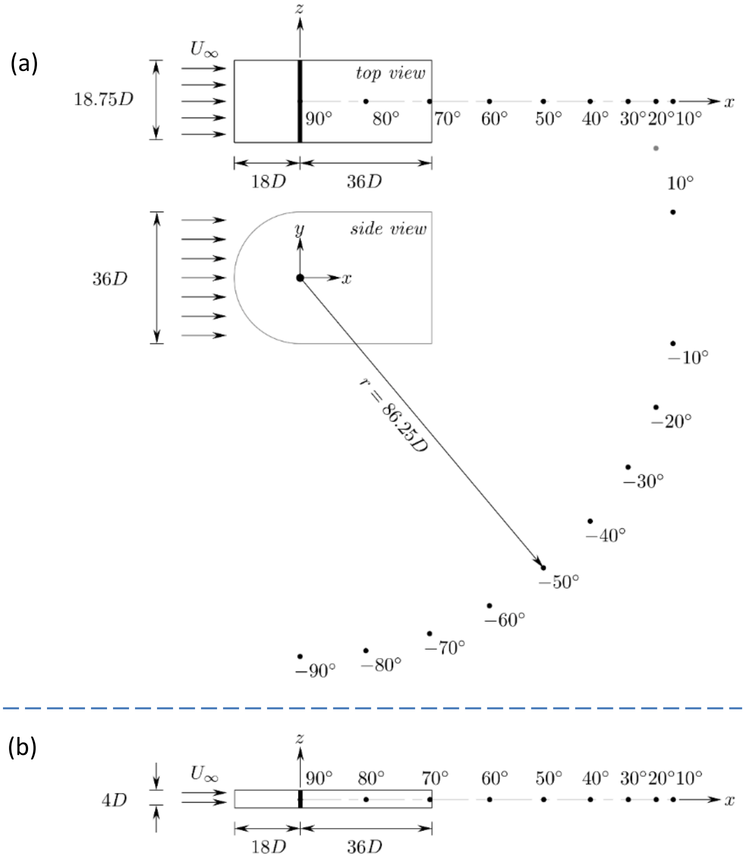

Figure 1: Schematic of the computational domain for (a) the full-span cylinder simulation; and (b) the top view of the reduced span simulation. Note that the side view and microphone layout of the reduced-span simulation are the same as those shown in (a), and although not shown in the side view, the microphones at positive angles (20º – 90º) are at the same locations as the equivalent negative angles, but mirrored about the $y = 0$ plane.

3 RESULTS AND DISCUSSION

3.1 Hydrodynamic results

Table 1 shows comparisons between global flow variables calculated from the full-span simulation and the equivalent values from experiments. The standard deviation of the lift force from the simulations ($C_{l_{rms}} = 0.297$) is in excellent agreement with the experimental value of 0.300 (Schewe, 1983). The calculated value of the mean drag coefficient ($C_d = 1.27$) differs from the experimental value of 1.13 by 12% (Schewe, 1983). The base suction coefficient ($-C_{pB} = 1.24$) is in good agreement with the experimental value of 1.2 (Williamson, 1996). The vortex formation length, which corresponds to the length of the recirculation region behind the cylinder, $l_F = 1.23D$, is within 17% of the experimental value presented in (Szepessy & Bearman, 1992). The calculated Strouhal frequency, $St = 0.193$, compares well with the experimental value of 0.200.

Table 1: Global flow variables calculated from the full-span simulation compared to values from experiments.

Variable	LES	Experimental
$C_{l_{rms}}$	0.297	0.300 (Schewe, 1983)
C_d	1.27	1.13 (Schewe, 1983)
$-C_{pB}$	1.24	1.20 (Williamson, 1996)
l_F/D	1.23	1.50 (Szepessy & Bearman, 1992)
St	0.193	0.200 (Casalino & Jacob, 2003)

Figure 2 shows the fluctuating lift and drag forces induced on both the full- and reduced-span cylinders by alternate shedding of vortices into the wake in the simulations. The highly three-dimensional nature of the flow over the full-span cylinder is evident from the low-frequency modulation of the fluctuating lift force, as shown in Figure 2(a). In contrast, it can be seen in Figure 2(b) that there is significantly less low-frequency modulation of the lift force on the reduced-span cylinder. This is a result of the periodic boundary conditions in the reduced-span simulation, which promote more coherent spanwise flow structures.

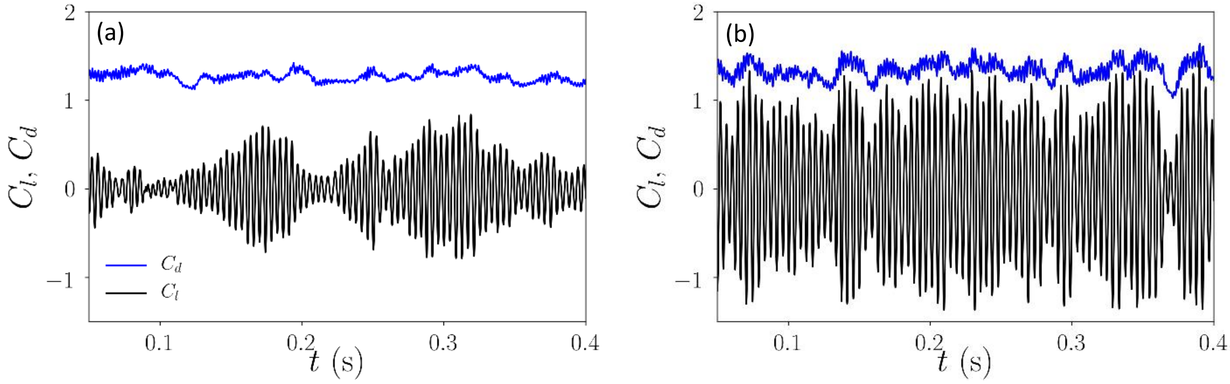

Figure 2: Time series of lift and drag coefficients from (a) Full-span, and (b) reduced-span cylinder.

Figure 3 shows the variation in lift force per unit span across the length of the full-span cylinder over a time interval of 0.15 s calculated from the simulation. This figure clearly shows the large variation in lift force acting on the cylinder with respect to time and position. The lift force is not perfectly in phase along the cylinder span, as evidenced by the line tracing out the meandering of the peak lift force. Regions where large sections of the cylinder experience high amplitude forcing at approximately the same time are highlighted. The acoustic pressure radiated by these sections of the cylinder will be largely in phase and will result in amplification of the far-field acoustic pressure. Regions where large sections of the cylinder experience low amplitude forcing are also shown. These regions delineate the spanwise location where the local lift force changes phase. The acoustic pressure radiated by the cylinder at these times will experience destructive interference which will result in an amplitude reduction.

The spanwise coherence function, Γ, and correlation coefficient, ρ, plotted as functions of η_d (where η_d is the non-dimensional spanwise separation distance) are shown in Figure 4(a) and (b), respectively. Definitions of both Γ and ρ are provided by Casalino & Jacob (2003). Data from the simulations and the experiment are fitted to Gaussian functions of the form $exp(-\eta_d^2/2L_g^2)$. For the coherence function, the best fit to the simulation data occurs with $L_g = 3.3$, whereas the experimental data is best fitted with $L_g = 4.7$. Similarly, the simulated correlation coefficient is best fit with a length scale of $L_g = 2.7$, with the experimental data best fit with $L_g = 6.6$. This shows that both the spanwise coherence and correlation of the surface pressures are under predicted in the full-span simulation. This will affect the magnitude of the sound pressure levels recorded in the far field, as shown in the following section.

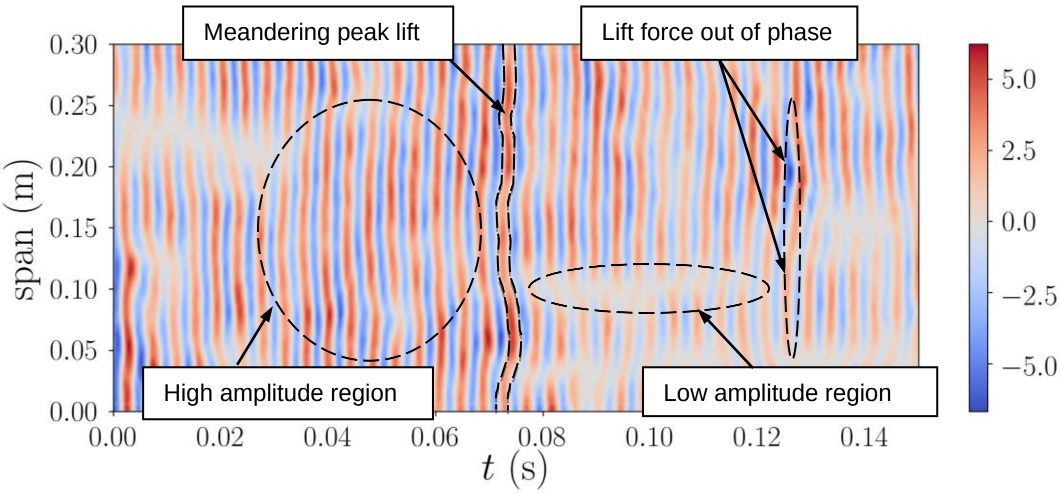

Figure 3. Lift force per unit span (N/m) acting on the simulated full-span cylinder over 0.15 seconds.

For the reduced-span cylinder, an estimate of the spanwise correlation length is extracted from the simulation results at each frequency. The spanwise correction to the far-field sound proposed by Seo and Moon (2007) is then applied. This is performed by a curve fitting technique, whereby the spanwise coherence function, Γ, is calculated for the reduced span model at each frequency. The spanwise coherence function for a cylinder undergoing vortex shedding is well approximated by a Gaussian function of the form $exp(-r^2/L_c^2)$, where L_c is the coherence length scale, and r is the spanwise separation distance (Seo & Moon, 2007). The curve fitting is achieved by locating the separation distance that corresponds to the first minimum of the coherence function, r_{min}, and calculating the length scale as

$$L_c(f) = \sqrt{\frac{-(r_{min}^2)}{\ln \Gamma_{ij}(r_{min},f)}} \tag{1}$$

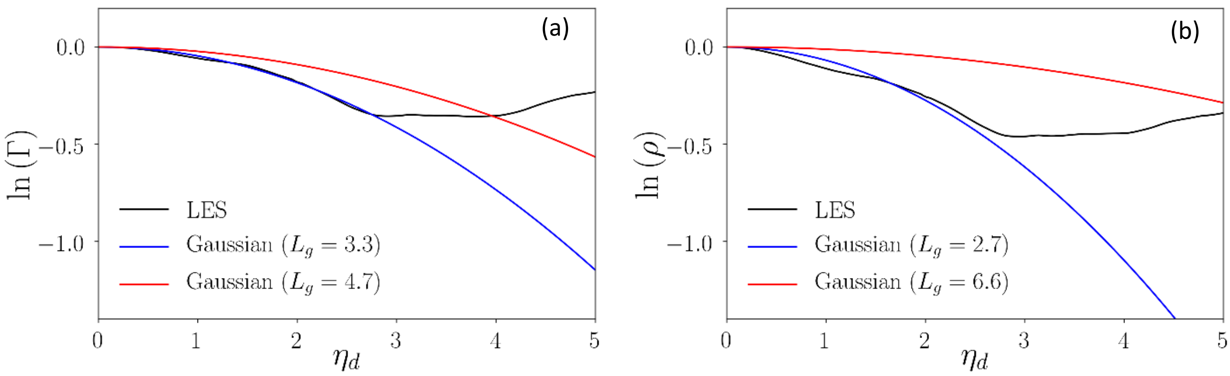

Figure 4: (a) Spanwise coherence function, Γ, at the vortex shedding frequency; and (b) spanwise correlation coefficient, ρ, as a function of non-dimensional length, η_d. Black lines are the simulation results. Red lines are curve fits based on length scales, L_g, obtained from the measurements of Casalino & Jacob (2003). Blue lines are curve fits based on length scales estimated from the present simulation results.

The variation of the spanwise coherence length scale (predicted using Equation (1) for the reduced-span cylinder) with frequency is shown in Figure 5. The spanwise coherence length scale at the vortex shedding frequency is predicted to be less than the length scale at the second harmonic of the vortex shedding frequency. This unexpected observation is due to the periodic boundary conditions used in the reduced-span simulation. The periodic boundary conditions restrict resolution of independent coherence lengths to separations of less than $2D$ (half the spanwise extent of the domain), which may apply artificial constraints on the spanwise coherence function used to compute Equation (1).

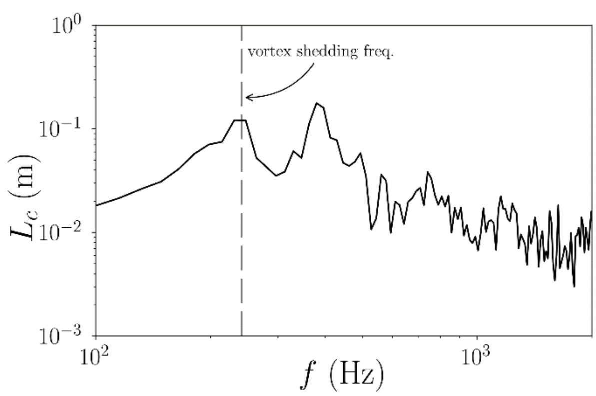

Figure 5: Variation in spanwise coherence length, L_c, with frequency, f, for the reduced-span cylinder simulation. The dashed vertical line shows the vortex shedding frequency.

3.2 Acoustics results

Figure 6 shows the acoustic sound pressure level (SPL) at various observation angles around the cylinder for the full- and reduced-span simulations, and the experimental values from Casalino & Jacob (2003). It should be noted that the measured data is unreliable below a frequency of 150 Hz as the jet noise and installation effects dominate the sound at these frequencies (Casalino, 2002). Also, at frequencies above approximately 1000 Hz, the background noise of the experimental facility contaminates the measured flow generated noise (Casalino & Jacob, 2003).

The reduced-span SPL results have been corrected according to the method derived in (Sea & Moon, 2007). In this, the SPL correction, $SPL_c(f)$, to be applied at each frequency, f, of the reduced-span far-field SPL is:

$$SPL_c(f) = \begin{cases} 10\log_{10}(N) & \frac{L_c(f)}{L_s} \leq \frac{1}{\sqrt{\pi}} \\ 10\log_{10}\left(\frac{L_c(f)}{L_s}\right) + 10\log_{10}\left(\sqrt{\pi}N\right) & \frac{1}{\sqrt{\pi}} < \frac{L_c(f)}{L_s} < \frac{N}{\sqrt{\pi}} \\ 20\log_{10}(N) & \frac{L_c(f)}{L_s} \geq \frac{N}{\sqrt{\pi}} \end{cases} \quad (2)$$

where N is the number of reduced span segments that fit into the full span and L_s is the simulated span.

A prominent peak at $f_0 = 250$ Hz is evident at each observation angle in the experimental data. The peaks at the vortex shedding frequency, f_0, and its third harmonic, $3f_0$, are generated by the unsteady lift induced on the rod by the Karman vortex street. The peak at the second harmonic, $2f_0$, is due to the fluctuating drag force on the cylinder and is most evident at microphones away from the azimuthal position at $\theta = 90^o$, with the magnitude of the peak increasing towards $\theta = 0^o$. This is consistent with the fact that the oscillations in lift force occur at the vortex shedding frequency while oscillations in drag force occur at twice the vortex shedding frequency. All peaks show a significant amount of broadening around the harmonic frequencies due to the three-dimensional nature of the vortex shedding process.

The vortex shedding frequency for the full-span simulation occurs at $f_0 = 241$ Hz, and the third harmonic occurs at 732 Hz. These values are 3.6% and 2.4% different to the corresponding experimental values. The peak from the second harmonic occurs at 489 Hz, which is 2.2% different to the experimental value. The frequencies of these tonal peaks predicted by the reduced-span simulation are similar to those predicted by the full-span simulation.

The frequency resolution of the experimental data plotted in Figure 6 is 2 Hz. This is much lower than the frequency resolution of the LES data, which is 18.4 Hz (due to limited simulation time and the data processing procedure). This difference in frequency increment affects the resolution of the tonal peaks, especially the peak at the vortex shedding frequency. For a more direct comparison with the simulation data, the experimental data around the vortex shedding peak have been averaged across frequency bands consistent with the LES bandwidth. These averaged results are shown by the blue lines in Figure 6.

It is seen that while the full-span simulation results capture the location of the vortex shedding frequency, its harmonics, and the spectral broadening around these peaks well, they are consistently 3-6 dB below the experimental data. The corrected reduced-span data, however, agree well with the amplitude of the measured data (within 1-3 dB), and accurately predict the peak locations at all observation angles. This is especially true when compared to the averaged experimental data around the vortex shedding frequency. The under-prediction evident in the full-span results is most likely due to the limited simulation time, which is insufficient to fully resolve the low-frequency amplitude modulation. For both the full- and reduced-span simulations, the LES data were divided into 14 segments, each with a duration of 0.054 seconds and 50% overlap to calculate power spectral densities using the modified periodogram method of Welch (1967). In comparison, the experimental data was divided into 400 segments, each with a duration of 0.5 seconds. It is clear that the simulation data is not able to capture the statistical uncertainty in the flow due to the modulation. Significantly longer simulation time would be required to do so.

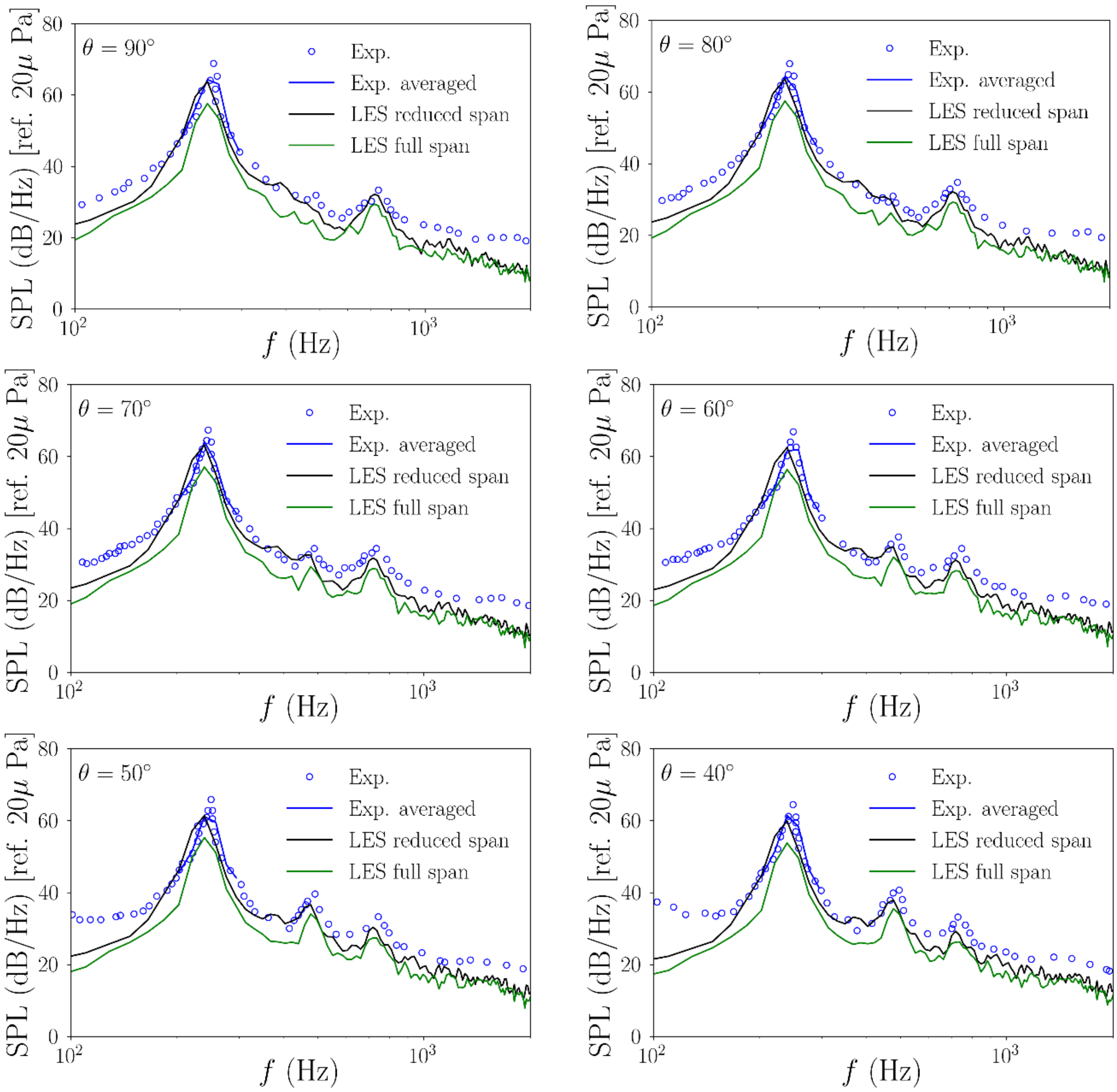

Figure 6: Power Spectral density of the radiated noise at a distance of 1.38 m from the cylinder mid-point at different observation angles. Circles represent the measurements of Casalino & Jacob (2003). Blue lines represent frequency averaging of experimental measurements to match numerical bandwidth. Black lines are the corrected SPL predictions from the reduced-span simulation. Green lines are the SPL predictions from the full-span simulation.

4 Conclusions

This study has investigated the accuracy of using LES with an acoustic analogy to predict the far-field acoustic signature produced by the flow around a circular cylinder at a Reynolds number based on cylinder diameter of 2.2×10^4. Numerical predictions of sound pressure level were compared to experimental data at a number of observation angles in the mid-span plane of the cylinder. Results from simulating the full-span cylinder matched the trend of the experimental SPL values, but were consistently 3-6 dB below the measured data. This underprediction was attributed to the low-frequency modulation of the fluctuating lift force on the cylinder (and consequently, the pressure on the cylinder surface and at the microphone locations), the full extent of which was not captured in the full-span simulation. It was shown that the run time required to capture the low-frequency modulation effect would be prohibitively long. Therefore, an alternative approach using a reduced-span cylinder was considered. A correction was used to scale the results from the reduced-span simulation to be comparable to the full-span experimental results. This resulted in improved agreement between the simulated and experimental results, particularly in the frequency range around the vortex shedding frequency. At other frequencies, the agreement between predicted and measured SPL was typically within 1-3 dB.

REFERENCES

Bensow, R. E. and Liefvendahl, M. An acoustic analogy and scale-resolving flow simulation methodology for the prediction of propeller radiated noise, *Proc. 31st Symp. Naval Hydrodynamics,* Monterey, California, 11-16 Sept., (2016).

Casalino, D. *Analytical and Numerical Methods in Vortex-Body Aeroacoustics*, Ph.D. Thesis, Politecnico di Torino and Ecole Centrale de Lyon, (2002).

Casalino, D. and Jacob, M. Prediction of aerodynamic sound from circular rods via spanwise statistical modelling, *Journal of Sound and Vibration*, **262**, 815-844, (2003).

Doolan, C. J. Computational bluff body aerodynamic noise prediction using a statistical approach, *Applied Acoustics*, **71**, 1194-1203, (2010).

Ffowcs Williams, J. E. and Hawkings, D. L. Sound generated by turbulence and surfaces in arbitrary motion, *Philosophical Trans. of the Royal Society London, Series A, Mathematical and Physical Sciences*, **264**(1151), 321-34, (1969).

Latorre-Iglasias, E., Thompson, D. J. and Smith, M.G. Experimental study of the aerodynamic noise radiated by cylinders with different cross-sections and yaw angles, *Journal of Sound and Vibration*, **362**, 108-129, (2016).

Liefvendahl, M. and Bensow, R. E. Simulation-based analysis of flow-generated noise from cylinders with different cross-sections, *Proc. 32nd Symp. Naval Hydrodynamics,* Hamburg, Germany, 5-10 August, (2018).

Nicoud, F. and Ducros, F. Subgrid-scale stress modelling based on the square of the velocity gradient tensor, *Flow, Turbulence and Combustion*, **62**, 183, (1999).

Schewe, G. On the force fluctuations acting on a cylinder in crossflow from subcritical up to transcritical Reynolds numbers, *Journal of Fluid Mechanics*, **133**, 265-285, (1983).

Seo, J. H. and Moon, Y. J. Aerodynamic noise prediction from long-span bodies, *Journal of Sound and Vibration*, **306**, 564-579, (2007).

Szepessy, S. and Bearman, P. W. Aspect ratio and end plate effects on vortex shedding from a circular cylinder, *Journal of Fluid Mechanics*, **234**, 191-217, (1992).

Williamson, C. H. K. Vortex dynamics in the cylinder wake, *Annual Review of Fluid Mechanics*, **28**, 477-539, (1996).

Welch, P. D. The use of fast Fourier transform for the estimation of power spectra: A method based on time averaging over short, modified periodograms, *IEEE Transactions on Audio and Electroacoustics*, **AU-15**(2), 70-73, (1967).

Weller, H. G., Tabor, G., Jasak, H., and Fureby, C. A tensorial approach to CFD using object oriented techniques, *Computers in Physics*, **12**(6), 620-631, (1998).